

INFLUENCE OF HEATING MODE ON THREE-DIMENSIONAL MANTLE CONVECTION

D. Bercovici, G. Schubert

Department of Earth and Space Sciences, University of California, Los Angeles

G. A. Glatzmaier

Earth and Space Sciences Division, Los Alamos National Laboratory

Abstract. Numerical models of three-dimensional, thermal convection in highly viscous spherical shells with different combinations of internal and basal heating consistently have upwelling concentrations in the form of cylindrical plumes and downwelling in planar sheets. As the proportion of internal heating increases, the number of upwelling plumes increases, and downwelling sheets become more vigorous and time-dependent. With any amount of basal heating, the entire convective pattern, during its evolution, is anchored to the upwelling plumes. As the proportion of internal heating increases, the heat flow carried by the upwelling plumes remains a large fraction of the basal heat flow. Downwelling sheets carry only a minor fraction (approximately 30%) of the basal heat flow (even when the shell is entirely heated from below), but they advect almost all of the internally generated heat. The relatively large number of plumes in the Earth's mantle (inferred from hotspots), the possibility that downwelling slabs are vigorous enough to penetrate the lower mantle, and the small fraction of terrestrial surface heat flow carried by plumes all suggest that the mantle is predominantly heated from within.

Introduction

Convective circulation in the Earth's mantle is distinctly three-dimensional and time dependent. No stronger evidence of this exists than in the very surface expression of mantle convection, i.e., plate tectonics with its diverse, migrating plate boundaries and wide distribution of hotspots. Indeed, the combination of three-dimensionality with sphericity in numerical simulations of mantle convection can account for some major features of plate tectonics: for a wide range of heating modes and a simple Newtonian rheology, planar sheets of downwelling and concentrated cylindrical plumes of upwelling are the basic forms of vertical transport (Bercovici et al., 1989a,b; Glatzmaier, 1988; Baumgardner, 1988), in agreement with the occurrence of descending slabs and plumes in the mantle. However, the lack of any active sheet-like upwelling in the numerical simulations correlates with evidence suggesting that mid-ocean ridges are passive features (Lachenbruch, 1976; Silver et al., 1988; Bercovici et al., 1989b).

Although sheet-like downwelling and cylindrical plume-like upwelling occur over a wide range of heating modes, convective patterns depend on the style of heating. The strength and number of upwelling plumes, the structure of sinking sheets and the nature of time dependence all change with heating mode. These effects of heating mode have particular significance for the Earth's mantle which is both heated from below by the hotter outer core and from within by radiogenic heat sources and secular cooling. While thermal histories indicate that the mantle is 70% to 80% internally heated (Schubert et al., 1980; Davies, 1980), recent high pressure diamond-anvil and shock experiments (Williams et al., 1987) on

the melting temperature of iron imply a much higher core-mantle boundary temperature than previously believed, and hence a possibly even greater component of basal heating. Given the uncertainty in the heat source for mantle convection, we seek to determine, through numerical simulations of three-dimensional convection in a spherical shell, whether the character of the convective flow itself bears some signature of the heating mode.

Numerical Model

We solve the three-dimensional, infinite Prandtl number, anelastic equations of mass, momentum and energy conservation in a self-gravitating spherical shell with an inner to outer radius ratio of 0.55, characteristic of the Earth's whole mantle (Glatzmaier, 1988; Bercovici et al., 1989a, b). The top and bottom boundaries of the shell are impermeable and shear stress free and the upper boundary of the shell is isothermal. With basal heating, the bottom boundary is also isothermal; when the shell is only heated from within, the lower boundary is insulated.

We solve for perturbations to a hydrostatic, adiabatic reference state based on the Murnaghan equation which prescribes a linear dependence of bulk modulus on pressure (Murnaghan, 1951; Glatzmaier, 1988). The dissipation number Di (the ratio of shell thickness d to adiabatic temperature scale height) is not constant in this formulation; its radial average $\overline{Di} = \ln(\bar{T}_{bot}/\bar{T}_{top})$ is approximately 0.5 (where \bar{T}_{bot} and \bar{T}_{top} are the bottom and top temperatures of the adiabatic reference state) as in the Earth's whole mantle. The Grüneisen parameter $\gamma = d(\ln \bar{T})/d(\ln \bar{\rho})$ (where $\bar{\rho}$ and \bar{T} are, respectively, the adiabatic reference state density and temperature) is constant at unity as is approximately true in the Earth's interior. Specific heat at constant pressure c_p , thermal conductivity k , dynamic viscosity η , and rate of internal heating ϵ (in units of power per unit mass) are all constant.

The conservation equations are solved by a spectral transform, Chebyshev-collocation method (Glatzmaier, 1984). Dependent variables are expanded in terms of spherical harmonics (for latitudinal and longitudinal dependences) and Chebyshev polynomials (for radial dependence). Accuracy of the spatial representation is assured by a drop of four orders of magnitude or more with decreasing wavelength in the power spectra of the dependent variables. Time integration is performed via finite differences: linear terms are treated implicitly with a Crank-Nicolson scheme and nonlinear terms are treated explicitly with an Adams-Bashforth method. Time steps are constrained to satisfy the Courant condition.

Four different modes of heating are considered. Cases I and II are for the spherical shell heated only from below and only from within, respectively. Cases III and IV are 50% and 80% heated from within, respectively; the proportion of internal heating is $1 - \langle q \rangle_{bot} / \langle q \rangle_{top}$ where $\langle q \rangle$ is the total heat flow (in units of power) through a boundary of the shell. The Rayleigh number Ra (a nondimensional measure of convective vigor) of all four cases is $Ra \approx 100 Ra_{cr}$ (where Ra_{cr} is the Ra for the onset of convection), about an order of magnitude below the likely range of

Copyright 1989 by the American Geophysical Union.

Paper number 89GL00806.

0094-8276/89/89GL-00806\$03.00

Ra for the Earth's whole mantle. Three additional nondimensional parameters are the same for all four cases; they are $\frac{4\pi c_p \bar{\rho}_{bot} d}{y_{bot}} = 1.26$, $\frac{c_p \bar{T}_{bot}}{g_{bot} d} = 0.12$, and $\bar{K}' = 3.5$, where g_{bot} is the gravity at the bottom of the shell (due to the core) and \bar{K}' is the slope of the linear relation for bulk modulus as a function of pressure. The amount of superadiabaticity is controlled by $\frac{\Delta T_{sa} + \bar{\rho}_{bot} \epsilon d^2/k}{T_{bot}}$ (where ΔT_{sa} is the superadiabatic temperature drop) which equals 1, 13.9, 2.4, and 14.9 for cases I – IV respectively. The relative amounts of heating are controlled by $\frac{\Delta T_{sa}}{\Delta T_{sa} + \bar{\rho}_{bot} \epsilon d^2/k}$ which equals 1, 0, 0.14, and 0.07 in cases I – IV, respectively.

Cases I – III have been partially discussed in Bercovici et al. (1989b). Here we present new results for a heating mode possibly characteristic of the Earth, and describe the advective heat transport and changes in convective patterns with depth and time.

Three-Dimensional Planform and Pattern Evolution

The convective pattern of case I (heating only from below) is characterized by narrow cylindrical plumes of upwelling surrounded by a weaker (i.e., lower velocity and less concentrated) interconnected network of downwelling sheets (see Cover top half). The upwelling plumes maintain their concentration and structure throughout the entire shell. However, the weaker downwelling is most sheet-like in the upper half of the shell; in the lower half of the shell, the sheets disintegrate as they diverge into the bottom boundary layer (Cover top left).

Although as many as six upwelling plumes occur early in the calculation of case I, the solution slowly evolves to a state with one major plume (in the eastern hemisphere) separated from two smaller plumes (Cover top right). The reduction in plume number occurs by fusion of plumes at their bases. Once this final state is reached the two smaller plumes in the western hemisphere continue to alternately approach and recede from one another. The temporal evolution of the solution is controlled by the drift of the plumes; i.e., the convective pattern is anchored to the strong upwelling plumes.

Calculations similar to case I but for a Boussinesq fluid (Bercovici et al., 1989a) yield regular polyhedral patterns with six and four plumes that are stable at least up to $Ra = 100Ra_{cr}$. The time dependence and lack of any polyhedral symmetry in case I may either be due to a difference in initial conditions from the Boussinesq cases or to the addition of compressibility. The anelastic conservation equations contain added nonlinearities that may break the regular polyhedral symmetry of the Boussinesq equations. Compressibility also weakens the downwelling sheets because adiabatic and viscous heatings warm downwelling regions and reduce their negative buoyancy; this may facilitate the coalescence of plumes (because the downwelling sheets are easier to breach).

Case II (heating only from within) has a horizontal convective pattern dominated by one very long downwelling sheet (in the western hemisphere) and several small cylindrical downwellings embedded in a broad weak background of upwelling (Cover bottom half). There is no well defined upwelling structure because there is no lower thermal boundary layer from which narrow instabilities can arise. Unlike case I, downwelling zones in case II maintain their structure and concentration as they approach the bottom boundary (Cover bottom left).

While the evolution of the convective pattern in case I is controlled by the drift and fusion of upwelling plumes, the pattern of case II evolves with no apparent end state (Cover bottom right). Although the long downwelling sheet drifts and bends, it is very long lived (persisting throughout the entire simulation). The downwelling plumes are, by comparison, transient features.

Case III (50% heating from within) is similar in planform to case I (Figure 1). However, the radial velocities of the upwelling cylindrical plumes and downwelling planar sheets are comparable. With internal heating, the thermal boundary layers have roughly equal temperature drops, hence the buoyancies of upwelling and downwelling regions are comparable. As in case I, upwellings conserve their plume-like structure as they traverse the shell. However, the downwelling sheets, while undergoing some dispersion as they approach the bottom boundary, maintain their coherence more than in case I (Figure 1a).

The convective pattern of case III evolves in the same manner as that of case I (Figure 1b). Upwelling plumes again tend to coalesce and reduce their number. Even with internal heating, the existence of strong upwelling plumes controls the time-dependent nature of the convective planform; plumes anchor the rest of the pattern to their own slow drift. However, the minimum number of plumes achieved is greater than for case I; case III finally has four separated plumes while case I has three plumes, two of which are very close to one another. The intensity and coherence of the downwelling sheets in case III are greater than in case I. Hence it is more difficult for the upwelling regions to breach the sheets as they attempt to fuse.

The convective pattern of case IV (80% heating from within) resembles that of case II, except that the upwelling regions are more well defined (Figure 2). Downwelling is again in the form of sheets and cylinders, while upwelling takes place in many (on the order of ten) small cylindrical plumes. As in case III, upwelling and downwelling velocities are comparable and the downwelling sheets maintain their integrity as they approach the bottom of the shell (Figure 2a). Downwelling sheets in case IV are relatively short-lived and display a very chaotic evolution. Although it is difficult to follow the pattern evolution in Figure 2b, more detailed analysis of the results shows a continuous formation and dispersal of downwelling sheets. While the upwelling plumes grow and diminish in vigor, they do not migrate significantly; even with a small amount of basal heating, the convective pattern remains essentially anchored to the upwelling plumes.

Heat Flow

Any amount of basal heating results in cylindrical plumes of upwelling. However, do the plumes only advect heat entering through the bottom of the shell or do they also carry heat generated internally? The best measure of a plume's heat flow is its advective heat flow near the middle of the shell (Glatzmaier, 1988). The net advective heat flow across a spherical surface at some radius r_o for compressible flow is

$$\bar{\rho}(r_o) \bar{T}(r_o) r_o^2 \int_0^{2\pi} \int_0^{\pi} u_r(r_o, \theta, \phi) S'(r_o, \theta, \phi) \sin \theta d\theta d\phi \quad (1)$$

where u_r is the radial velocity, S' is the nonspherically symmetric part of the specific entropy, θ is colatitude, and ϕ is longitude; S' is used instead of the total entropy because, by conservation of mass, the net advection of any spherically symmetric quantity through a concentric spherical surface is zero. An estimate of the heat flow carried upwards by a plume can be made by integrating $\bar{\rho} \bar{T} u_r S'$ over the horizontal cross-sectional area of the plume at $r_o = 0.77r_{top}$ (i.e., at a radius midway through the shell).

The last time frame of case I (Cover top right) has three upwelling plumes (the middle plume has a minor plume-like appendage) The total heat flow (in units of power) advected by these plumes is approximately 70% of the total heat flow through the shell. The final state of case III has four upwelling plumes (Figure 1b). The total advective heat flow carried by all of these plumes

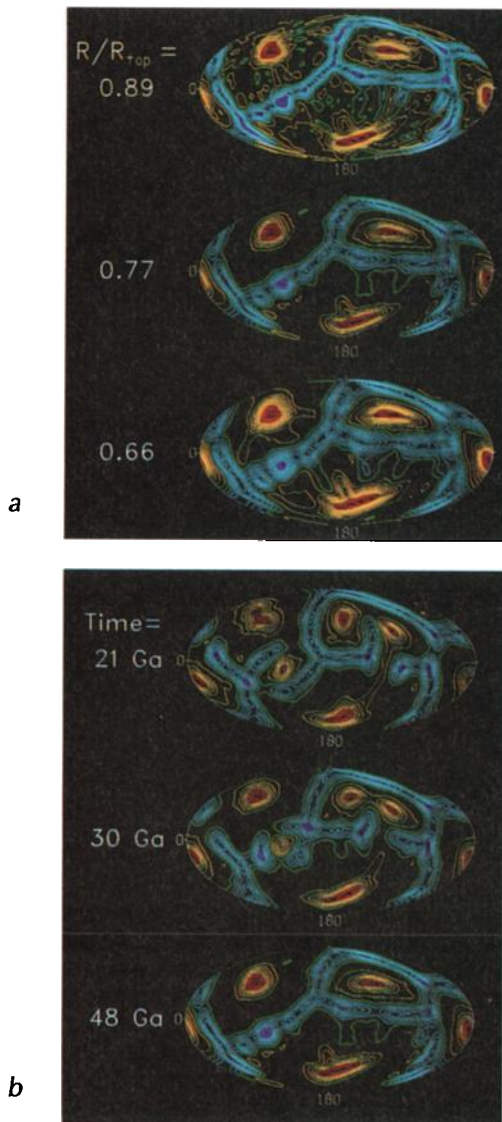


Fig. 1. Contours of radial velocity w on a spherical surface at *a*) different depths for one time, and *b*) different times for one depth (at $r/r_{top} = 0.77$) for case III (in which the shell is 50% heated from within). The images are in an equal area projection. Colors represent equal intervals of velocity. Red contours are for w in the range $|w|_{max} \geq w > \frac{1}{2}|w|_{max}$; yellow is for $\frac{1}{2}|w|_{max} \geq w > 0$; green is for $w = 0$; cyan (light blue) is for $0 \geq w > -\frac{1}{2}|w|_{max}$; blue is for $-\frac{1}{2}|w|_{max} \geq w > -|w|_{max}$. All colors appear in these frames because the upwelling and downwelling velocities are comparable.

midway through the shell is approximately 80% of the total heat flow into the base of the shell, or 40% of the total heat flow out of the shell. Case IV has a broad distribution of relatively weak upwelling plumes; there are about 10 plumes at any one time. At the $84Ga$ time frame (bottom of Figure 2b), the total heat flow carried by the plumes is approximately 60% of the total bottom heat flow and 12% of the total heat flow out of the shell. The plumes of cases III and IV carry no more heat at $r_o = 0.89r_{top}$ (i.e., at a depth of 25% of the shell thickness) than they do at $r_o = 0.77r_{top}$, implying that they are not significantly affected by the internal heating. These values of plume heat flow are only approximate since the estimates for plume heat flow are rough and all the solutions are time dependent.

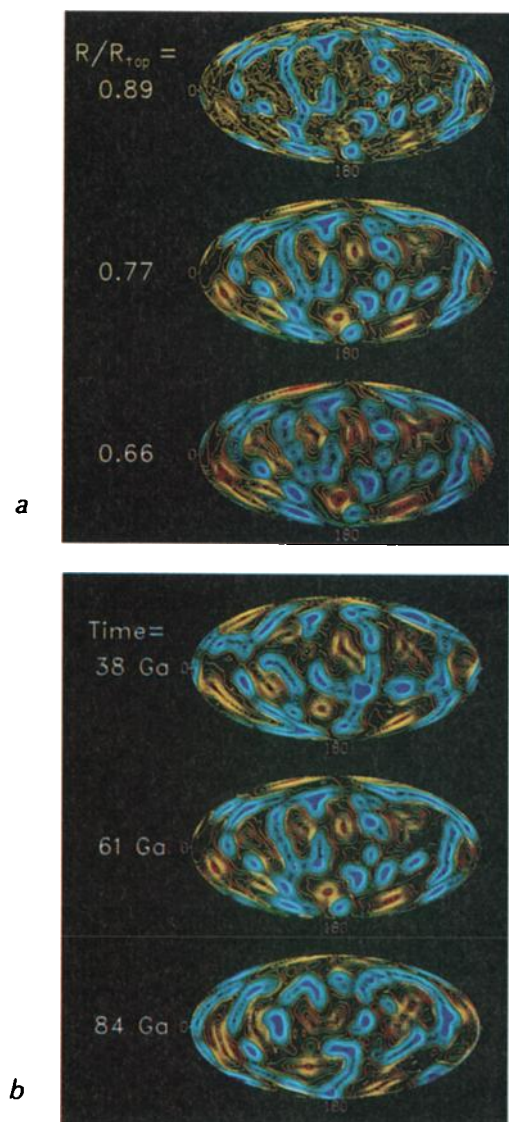


Fig. 2. Same as Figure 1, but for case IV (in which the shell is 80% heated from within). As in Figure 1, all colors appear in these frames because the upwelling and downwelling velocities are comparable.

Since downwelling sheets have negative u_r and S' , they also carry a portion of the net heat flux; i.e., they cool the shell by injecting "cold" material into it. In cases I, III and IV, cylindrical concentrations of downwelling individually carry between an order of magnitude less (case I) and an order of magnitude more (case IV) heat flow than any individual upwelling plume. One can estimate the heat flow carried by the downwelling sheets by assuming that radial heat conduction is negligible midway through the shell; this assumption is valid when the heat input into the shell is greater than the heat that can be conducted along the adiabat, i.e., when $\Delta T_a < \Delta T_{sa} + \bar{\rho}_{bot} \epsilon d^2 / k$ (where ΔT_a is the adiabatic temperature drop across the shell and is approximately equal to $\overline{Di} \bar{T}_{bot}$), as is true in this paper (Glatzmaier, 1988; Bercovici, Schubert and Glatzmaier, work in progress). The downwelling sheets carry approximately 30%, 60%, and 90% of the total heat flow out of the shell in cases I, III and IV, respectively. In all three cases, the weak background flow carries almost no heat flux and in fact has pockets of negative heat flow where cold (hot) material is being entrained by strong upwelling (downwelling) currents. In cases III and IV, with internal

heating, downwelling sheets play the major role in the advection of heat.

Discussion and Conclusions

Although these numerical models lack much of the reality of the Earth's mantle (e.g., higher Rayleigh numbers, variable viscosity, discontinuities from phase and/or compositional changes), their display of Earth-like features (planar descending slabs, cylindrical upwelling plumes) is a strong measure of the importance of three-dimensional flow in spherical geometry. Cylindrical upwelling plumes (and by inference, hotspots) are the signature of basal heating. Plumes carry about 60% to 80% of the heat supplied through the bottom boundary. Heat flow carried by plumes is therefore representative of the proportion of basal heating. Estimates of plume heat flow from convectively generated topography (Davies, 1988) indicate that mantle plumes carry no more than about 10% of the Earth's total surface heat flow. This closely corresponds to case IV, implying that the mantle is approximately 80% internally heated, in agreement with estimates from thermal history modelling (Schubert et al., 1980). The results of this study also suggest that downwelling slabs transport most of the heat across the mantle.

The durability of descending slabs is strongly dependent on the heating mode of the mantle. In case I (heating entirely from below), the downwellings have weak velocities relative to the upwellings, and the downwelling sheets disperse near the bottom boundary. With internal heating (cases II through IV), the downwellings are more vigorous and better able to maintain their structure as they impinge on the bottom boundary. Therefore, a large percentage of internal heating greatly increases the survivability of a sinking slab. Whether downwelling slabs in the Earth's mantle maintain their structure as they descend is a matter of speculation. Analyses of seismic travel time anomalies of deep focus earthquakes (Creager and Jordan 1984, 1986; Fischer et al., 1988) suggest that slabs penetrate into the lower mantle, breaching the chemical or phase-transition barrier that separates the upper mantle from the lower mantle at a depth of approximately 670 km. There is also a significant correlation between seismically and gravitationally inferred depressions in the core-mantle boundary (CMB) with the circum-Pacific trenches and descending slabs (Dziewonski, 1984; Hager et al., 1985; Dziewonski and Woodhouse, 1987; Morelli and Dziewonski, 1987; see review by Silver et al., 1988). Thus, even if slabs do not reach the CMB, the stresses induced by their sinking motions are apparently felt at the base of the mantle. While temperature-dependent viscosity would no doubt postpone the disruption of the slabs, a viscosity increase with depth could induce the break-up to occur sooner (by reducing the viscosity contrast between the slab and surrounding mantle).

The number of upwelling plumes also appears to be indicative of heating mode: an increase in the proportion of internal heating tends to cause an increase in the number of upwelling plumes (from 3 in case I to approximately 10 in case IV). The large number of hot spots at the Earth's surface therefore suggests a large component of internal heating in the mantle.

The calculations which are predominantly heated from within are most able to reproduce the style of convection in the Earth's mantle. Therefore, while hotspots indicate that there is a minor component of heating from the core, internal heating from the decay of radiogenic elements and secular cooling dominate.

Acknowledgments. The authors wish to acknowledge helpful discussions with participants of the Los Alamos Mantle Convection Workshop sponsored by the Institute of Geophysics and Planetary Physics. This work was supported by grant NAG5152 from NASA and a computing grant from the San Diego Supercomputer Center, SDSC. All computations and graphics were generated on a Cray XMP-48 at SDSC.

References

- Baumgardner, J. R., Application of supercomputers to 3-d mantle convection, in *The Physics of the Planets* (S.K. Runcorn, ed), John Wiley and Sons, New York, 199–231, 1988.
- Bercovici, D., G. Schubert, G. A. Glatzmaier, and A. Zebib, Three-dimensional thermal convection in a spherical shell, *J. Fluid Mech.*, in press, 1989a.
- Bercovici, D., G. Schubert, and G. A. Glatzmaier, Three-dimensional spherical models of convection in the Earth's mantle, *Science*, **244**, 950–955, 1989b.
- Creager, K. C., and T. H. Jordan, Slab penetration into the lower mantle, *J. Geophys. Res.*, **89**, 3031–3049, 1984.
- Creager, K. C., and T. H. Jordan, Slab penetration into the lower mantle beneath the Mariana and other island arcs of the north-west Pacific, *J. Geophys. Res.*, **91**, 3573–3589, 1986.
- Davies, G. F., Thermal histories of convective Earth models and constraints on radiogenic heat production in the Earth, *J. Geophys. Res.*, **85**, 2517–2530, 1980.
- Davies, G. F., Ocean bathymetry and mantle convection, 1. Large-scale flow and hotspots, *J. Geophys. Res.*, **93**, 10,467–10,480, 1988.
- Dziewonski, A. M., Mapping the lower mantle: Determination of lateral heterogeneity in P velocity up to degree and order 6, *J. Geophys. Res.*, **89**, 5929–5952, 1984.
- Dziewonski, A. M., and J. H. Woodhouse, Global images of the Earth's interior, *Science*, **236**, 37–48, 1987.
- Fischer, K. M., T. H. Jordan, and K. C. Creager, Seismic constraints on the morphology of deep slabs, *J. Geophys. Res.*, **93**, 4773–4783, 1988.
- Glatzmaier, G. A., Numerical simulations of stellar convective dynamos I. The model and method, *J. Comp. Phys.*, **55**, 461–484, 1984.
- Glatzmaier, G. A., Numerical simulations of mantle convection: Time-dependent, three-dimensional, compressible, spherical shell, *Geophys. Astrophys. Fluid Dyn.*, **43**, 223–264, 1988.
- Hager, B. H., R. W. Clayton, M. A. Richards, R. P. Comer, and A. M. Dziewonski, Lower mantle heterogeneity, dynamic topography, and the geoid, *Nature*, **313**, 541–545, 1985.
- Lachenbruch, A. H., Dynamics of a passive spreading center, *J. Geophys. Res.*, **81**, 1883–1902, 1976.
- Morelli, A., and A.M. Dziewonski, Topography of the core-mantle boundary and lateral homogeneity of the liquid core, *Nature*, **325**, 678–683, 1987.
- Murnaghan, F. D., *Finite Deformation of an Elastic Solid*, John Wiley, New York, 1951.
- Schubert, G., D. Stevenson, and P. Cassen, Whole planet cooling and the radiogenic heat source contents of the Earth and moon, *J. Geophys. Res.*, **85**, 2531–2538, 1980.
- Silver, P. G., R. W. Carlson, and P. Olson, Deep slabs, geochemical heterogeneity, and the large-scale structure of mantle convection: investigation of an enduring paradox, *Ann. Rev. Earth Planet. Sci.*, **16**, 477–541, 1988.
- Williams, Q., R. Jeanloz, J. Bass, B. Svendsen, and T. J. Ahrens, The melting curve of iron to 250 Gigapascals: Constraint on the temperature at the Earth's center, *Science*, **236**, 181–182, 1987.

D. Bercovici and G. Schubert, Department of Earth and Space Sciences, University of California, Los Angeles, CA 90024-1567
G. A. Glatzmaier, ESS-5 MS-F665, Los Alamos National Laboratory, Los Alamos, NM 87545.

(Received: January 31, 1989)

Revised: April 19, 1989

Accepted: April 21, 1989)